Numerical calculations of heat transfer during FC-72 flow in minichannels performed with ANSYS software

Kacper Kuta[1], *Magdalena* Piasecka[2,*], and *Slawomir* Blasiak[3]

[1,2,3] Kielce University of Technology, Faculty of Mechatronics and Mechanical Engineering
Al. Tysiaclecia Panstwa Polskiego 7, 25-314 Kielce, Poland

Abstract. The main aim of the paper was to apply numerical calculations in ANSYS software to solve problems related to steady-state convective heat transfer during FC-72 flow in a minichannel heat sink. A mathematical model of fluid flow in a minichannel heat sink was proposed. Data from research conducted on the experimental stand with asymmetrically heated test section were selected. The element cooled by fluid flowing in minichannels was a thin foil. The distribution of temperature on the outer heated foil surface was measured using infrared thermography. Thermocouples and pressure meters were installed at the inlet and outlet of the minichannels. A CAD model was prepared with respect to the geometry of the test section. The mesh was created in ANSYS Mesher. A suitable model of turbulences was selected and materials temperature dependencies were considered. The iterative process of creating the model and comparing the results obtained by the CFD calculation was used to capture the fluid behavior. The velocity magnitudes and temperature distributions were presented as the main results of numerical calculations.

1 Introduction

Extensive experimental and theoretical studies are required to understand the boiling phenomena in the group of small hydraulic diameter channels called micro- or minichannel heat sinks. The phase change which accompanying boiling processes allows the highest possible heat fluxes to be obtained at low temperature differences between the heated surface and the working fluid over a small heat transfer area. Scientific studies on heat transfer in cooling liquids flowing through a group of channels of small hydraulic diameters are being conducted intensively [1-9]. This topic is not popular in research mainly due to practical difficulties. The results concerning heat transfer in flows boiling in a group of mini- or microchannels are inconsistent, and even contradictory. The calculation methods of heat transfer determination in the flow boiling in a group of mini- or microchannels often represent only numerical simulations, which are not based on the results of own experimental studies, calculations are often based on the results of experimental results obtained by other researchers. It should be emphasized that the experiment is the most important aspect which contributed most to the direct describing of boiling heat transfer. It is especially significant for complicated heat transfer systems, in which the size of bubbles can be larger than the size of the channel because any forecasts on heat transfer are difficult under such circumstances.

Creating a coherent, predictable and accurate computational model of heat transfer during fluid flow through a minichannel is both a designer and a scientific challenge. Such a model, computationally simple and easy to use, would allow greater control over design of small-scale, effective heat exchangers. Sometimes it is necessary to build an experimental set-up for every design idea. A standardized model for a compact heat exchanger with minichannels of various geometries, created using numerical computing, would lead to reduction of design time in many practical applications.

Based on experimental data and analytical and analytical numerical methods with using Trefftz functions, the values of the heat transfer coefficient on the heating surface that contacts the fluid flowing in a minichannel were determined in earlier works [10-13]. Some attempts have been made to predict the behavior of cooling fluids [14, 15] flowing in minichannels due to numerical calculations. To verify CFD modeling, selected data from experiments were applied in numerical calculations using ANSYS CFX [14] and ADINA software [15]. It is worth mentioning that ANSYS CFX software, a computational fluid dynamics program, is often used to simulate and optimize fluid flow as in [16].

2 Experimental stand and methodology

In investigations conducted at the Kielce University of Technology, several experimental stands were built and furnished with equipment for investigation of flow boiling heat transfer in minigaps. The essential part of each stand is a test section of different geometries and spatial orientations. A view of the experimental stand with a test section with rectangular minichannels or an annular minigap is shown in Fig. 1.

*Corresponding author: tmpmj@tu.kielce.pl

Fig. 1. A view of the experimental stand with a test section with rectangular minichannels or an annular minigap.

A new experimental stand with a test section with a group of rectangular minichannels or microchannels is shown in Fig. 2

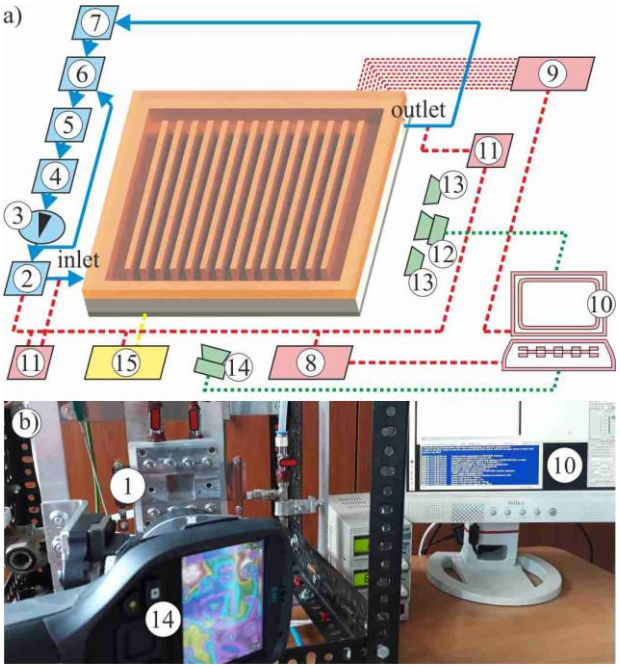

Fig. 2. The new experimental stand with a test section with a group of rectangular mini- or microchannels (a heat sink): a) a view, b) a schematic diagram; 1 – a test section, 2 – a mass flow meter, 3 – a circulating gear pump, 4 – a filter, 5 – a deaerator, 6 – pressure meter, 7 – plate-type heat exchanger, 8,9 – data acquisition station, 10 – a PC computer, 11 – a pressure meter, 12 – a high-speed camera, 13 – LEDs, 14 – an infrared camera, 15 – a power supply, 16 – a front cover, 17 – a group of mini- or microchannels, 18 – a channel body, 19 – an inlet/an outlet chamber, 20 – a glass, 21 – a heated foil.

In the flow loop, Fig. 2a, a cooling fluid (such as Novec 7200, 7100, 649, Fluorinert FC-72) is recirculated. The flow loop consists: a test section with a group of mini- or microchannels (a heat sink), a mass miniflow meter with a controller for flow stabilizing at the inlet to the test section, a circulating pump, a filter, a deaerator, a compensating tank/a pressure regulator, and a tube type heat exchanger, with water as a coolant. The data and image acquisition system, designed to collect the measurement data, includes data acquisition stations, an infrared camera and a high-speed camera with a PC computer with appropriate software. The lighting system comprises high power LEDs to provide light for the two-phase flow structures. The temperature and pressure of the working fluid of the fluid at the inlet and outlet of the test section are measured by thermocouples or pressure meters, respectively. The supply and control system contains a power supply unit and a shunt.

The essential part of the experimental stand is a replaceable test section with a group of rectangular mini- or microchannels. The test section view is shown in Fig. 3a and the transverse cross-section of the test section - in Fig. 3b. The number, width and length of the channels can vary. The heated element for working fluid flowing along minichannels is a thin mretal foil made of Haynes-230 alloy.

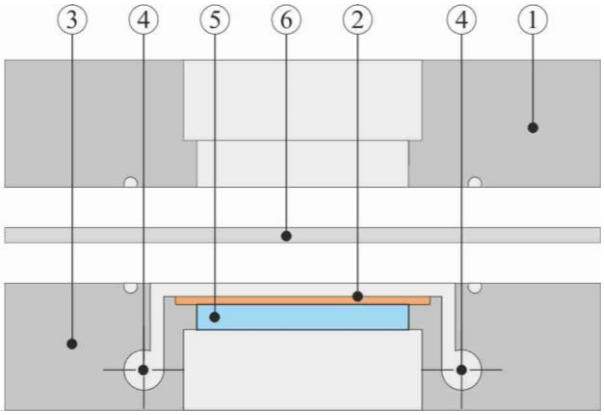

Fig. 3. A transverse cross-section of the test section with a minichannel heat sink, 1 – a front cover, 2 – a group of mini- or microchannels, 3 – a channel body, 4 – an inlet/an outlet chamber, 5 – a glass, 6 – a heated foil.

During the experiment, after deaeration, there is a flow of the working fluid in the main loop of the experimental stand. The liquid at the temperature below its boiling point flows in the test section. The heat flux supplied to the heated foil is gradually increased by adjustment of supplied heating power until developed nucleate boiling occurs. The schematic diagram of the fluid flow in the test section with a channel heat sink is shown in Fig. 4.

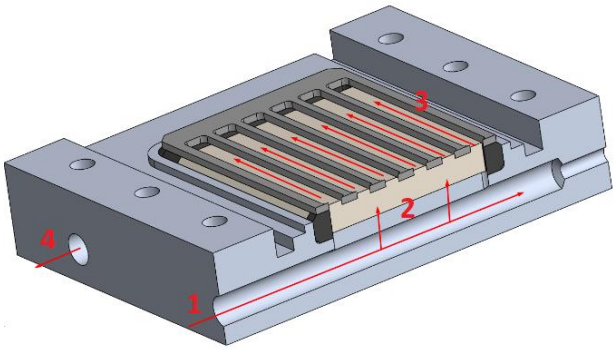

Fig. 4. The schematic diagram of the fluid flow in the test section with a minichannel heat sink, 1 – an inlet collector, 2 – inlet to the channels, 3 – a singular minichannel, 4 – an outlet collector.

For the present work, several versions of a test section construction were created in CAD software. An overall construction of the test section is depicted in Fig. 5.

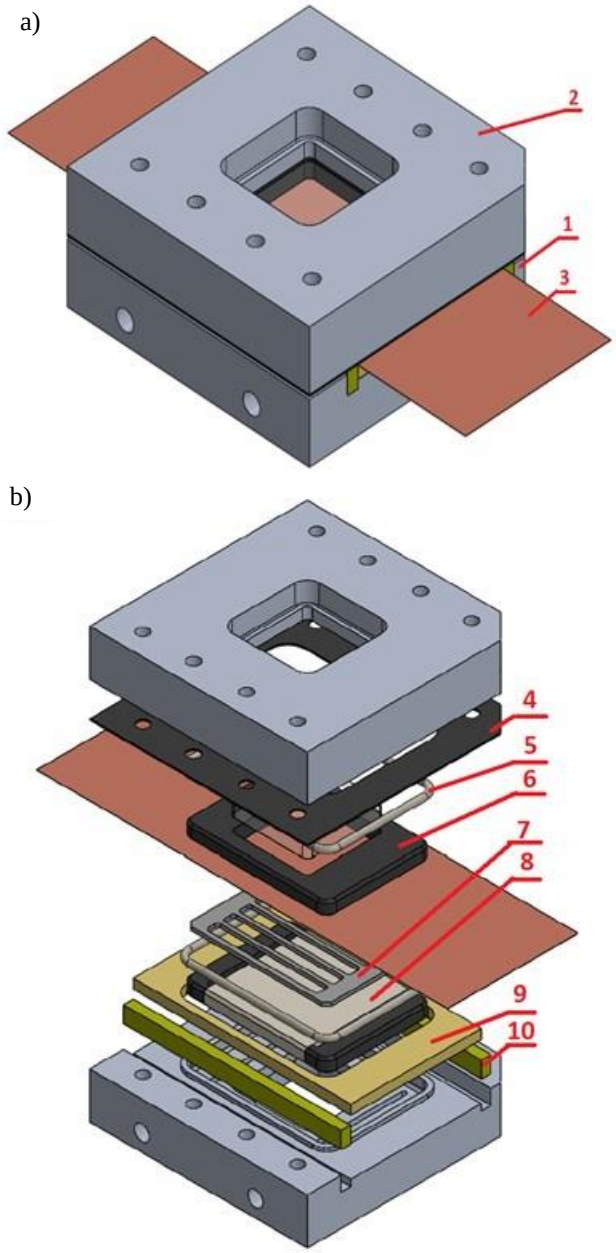

Fig. 5. An overall construction of the test section, 1 – upper body (a cover), 2 – bottom body half, 3 – heated foil, 4 – thin top insulation plate, 5 – top O-ring, 6 – thick insulation plate, 7 – minichannel plate, 8 – glass plate, 9 – bottom insulation, 10 – bottom insulation wedges.

Currently, the reduced CAD model is being built for CFD calculations. All measuring equipment and the environment outside the geometry of the test section were rejected to reduce a computational domain. Schematic diagrams of internal flow volume geometry were shown in Fig. 6. One of them was prepared for visualization purposes (Solid Works, Fig. 6a) and the other for numerical calculations (Design Modeler, an ANSYS module, Fig. 6b).

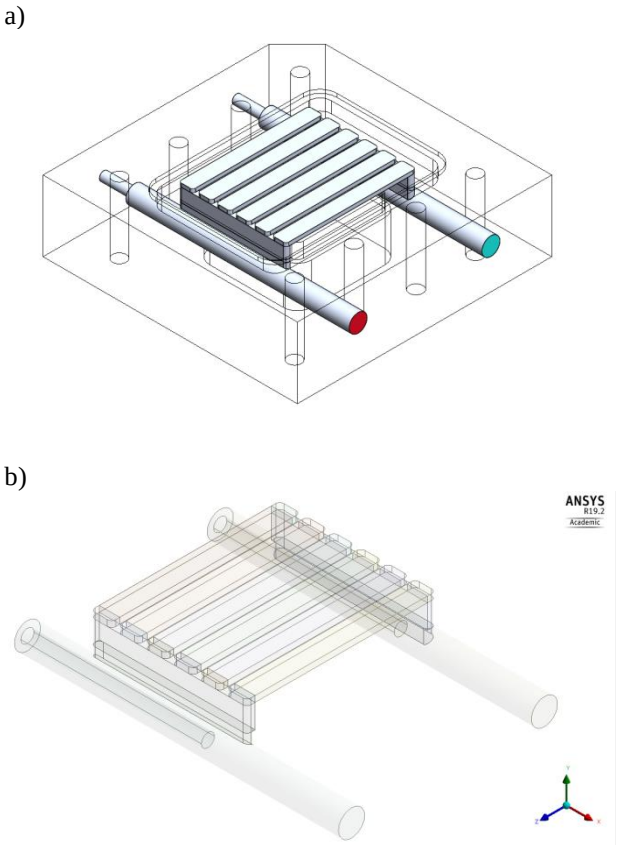

Fig. 6. Schematic diagrams of internal flow volume geometry created in programs: a) SolidWorks, b) Design Modeler, an ANSYS module.

3 Numerical calculations

3.1 Assumptions and calculation preparation

To simplify the problem, some assumptions were made. Most of them was considering incompressible flow with relatively low turbulence. Radiance was considered negligible and it was assumed that all properties of materials linearly changing with respect to temperature. No viscous heating effect was calculated. The fully developed flow at the inlet was considered.

In ANSYS, the Fluent SIMPLE algorithm was selected for solving (simplified) Navier-Stokes equations. For this algorithm, boundary conditions were applied. It was assumed that heat transfer through the walls is performed by conduction in materials according to Fourier's law.

Heat transfer in regions, exterior to computational domain, is treated as 1D (assuming the direction of heat transfer), for each wall separately. Each material has assigned its respective thermal conductivity that was taken directly from the manufacturers' data in tabular form with respect to temperature.

The fluid in a minichannel is heated through its top wall by a heated foil. It is considered uniformly heated with a heat flux value equal to 35 kW/m^2. Roughness parameters were assumed for the side walls of the

minichannel and heated foil. These data, coupled with the viscosity of the working fluid, were used initially to calculate the velocity profile and then heat transfer near the walls.

The main parameters of the experimental series taken for the calculations were as follows:

- overpressure at the inlet:139 kPa,
- overpressure at the outlet:130 kPa,
- fluid temperature in the inlet chamber: 294 K.

Changes in temperature outside of the computational domain were neglected. A standard SST model of turbulence for low Reynolds flows was assumed, with energy equations and pressure-velocity coupling. After few initial iterations (~150) to initialize calculations, a second order upwind was selected to stabilize a solution.

3.2 Mesh preparation

All meshes used were hexahedral because they are relatively easy to control and allow for high tolerance of big aspect ratio cells and fit the geometry. Characteristics of meshes was specified in Table 1. Meshes were refined with the inflation method with specified thickness of the first layer. Meshing of this object, performed in Mesher, was focused on altering the following parameters: global size, inflation direction, height of the first layer and growth rate.

Table 1. Details of mesh refinement.

Mesh No.	Global size [mm]	Geometry selection	First layer height [μm]	Max. layers	Growth rate	Nodes	Elements
1	1	Top surface	42.5	10	1.1	81209	71680
2	1	Top surface	4.25	40	1.05	224519	206080
		Bottom surface	20	5	1.1		
3	0.5	Top surface	4.25	20	1.05	499851	465920
		Bottom surface	20	5	1.10		
4	0.5	Top surface (+bias)	4.25	40	1.05	463239	427896
5	0.5	Top surface (+bias)	4.25	50	1.02	513264	487296

Meshes from No. 1 to No. 3, Table 1, were selected to the test to create a sufficiently dense boundary layer. In next attempts, the roughness of the border walls was taken into consideration to ensure a physically correct velocity profile biased sizing toward the aluminum walls, Fig. 7.

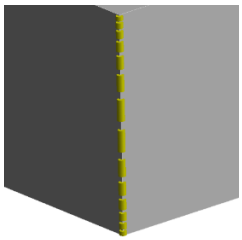

Definition	
Suppressed	No
Type	Element Size
Element Size	0.125 mm
Advanced	
Behavior	Soft
Growth Rate	Default (1.2)
Capture Curvature	No
Capture Proximity	No
Bias Type	_ ___ _____ ___ _
Bias Option	Bias Factor
Bias Factor	5.0

Definition	
Suppressed	No
Type	Element Size
Element Size	0.25 mm
Advanced	
Behavior	Soft
Growth Rate	Default (1.2)
Capture Curvature	No
Capture Proximity	No
Bias Type	_ _ ___ _____
Bias Option	Bias Factor
Bias Factor	5.0
Reverse Bias	No Selection

Fig. 7. Bias details.

After reaching the ANSYS Educational limit of 512k nodes + elements, another simplification was assumed for mesh No. 5 – singular minichannel symmetry plane. For the last mesh, only half of the geometry was considered. To use an additional quota of cells + elements, an increased bias strategy was added to increase the density of cells toward surfaces in contact with heated foil (‘top surface’), the aluminum wall (‘outer surface’) and the glass plate (‘bottom surface’).

A cross-section and isometric view of the final mesh (No. 5, Table 1) is shown in Fig. 8. There was no significant difference between the results obtained with using meshes No. 4 and No. 5 which means reaching mesh independent solution.

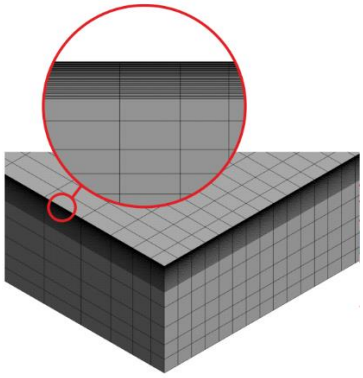

Fig. 8. Cross section of mesh No. 5.

The properties of the phase materials within the range of temperatures had to be considered during the calculation procedure. The heated foil was made of Haynes-230 alloy [17]. Fluorinert FC-72 (3M) [18] was the working fluid. Minichannel walls were made of aluminum (PA6) and typical glass material was selected for the glass panel. Following information provided by the manufacturers, the properties of all listed materials were loaded into the ANSYS Fluent program.

4 Results and discussion

The velocity magnitudes and temperature distributions are presented as the main results of numerical calculations. Planes selected for cross sections are symmetrical (for velocities) to compare numerically computed velocity profile with analytically computed average velocity obtained on the basis of the experimental data. For temperatures there is a top view showing first layer of fluid (contacting the heated foil), one solutions graph drawn on the facets of mesh, close to the end of the minichannel, and one view on cross section in the symmetry plane.

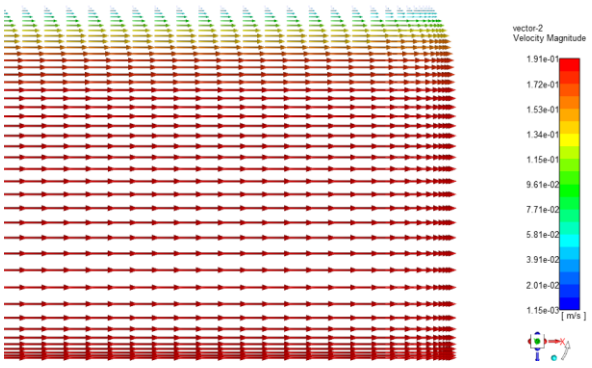

Fig. 9. Velocity magnitude profile parallel to ZX plane (a top view from the heated foil direction)

Analyzing the results obtained from calculations using the final dense mesh, a drop of velocity towards wall of the minichannel can be noticed, Fig. 9. This corresponds both with observable effects and analytical computations. Very crude cells in the middle of the image emphasize intense central flow and densely packed vectors close to the top and bottom have parabolic curve expected in such a setup. Moreover, the velocity magnitude vectors are almost constant on given depth up to last 10% width from side walls, where they parabolically decrease to reach minimal values of around 1.15e-02 m/s. From analytical calculations, an average velocity of approximately 0.12 m/s was expected (according to the experimental data). Since an average value close to that was obtained, the profile was considered physically feasible.

With changed global setting of mesh, more cells are generated in the middle of the flow, and a more pronounced parabolic profile also on top view. This barely affects maximum values of the velocity magnitude plot, but allows for the observation of the the distribution of velocity further from the top and bottom walls. The values on the top and bottom surfaces (Fig. 10) are close to 0 (0.04 m/s), which is consistent with the model. Minimal asymmetry, showing a difference of 0.15 m/s on the edges, shows small differences in roughness between the glass plate and the heated foil surfaces.

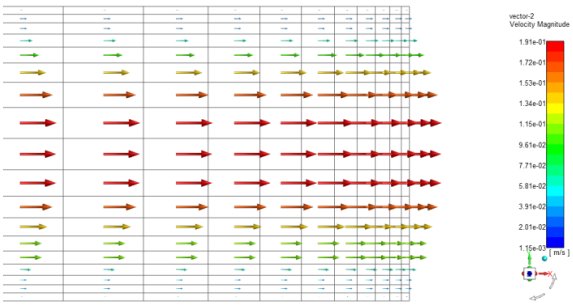

Fig. 10. Velocity magnitude profile parallel to XY plane (a side view from symmetry plane)

The static temperature distribution on the contact surface between the working fluid and the heated foil is illustrated in Fig. 11. Narrow stripes of hotter regions are observed along the whole minichannel (seen as red lines). Consistency of relative temperature of stripe and middle flow vary with different mesh densities.

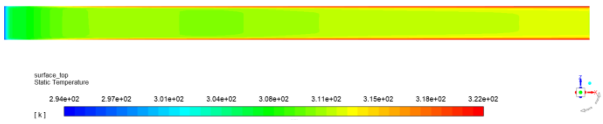

Fig. 11. Static temperature distribution on the contact surface between the working fluid and the heated foil.

An isometric view of the temperature distribution in the fluid up to the contact surface with the heated foil is presented in Fig. 12.

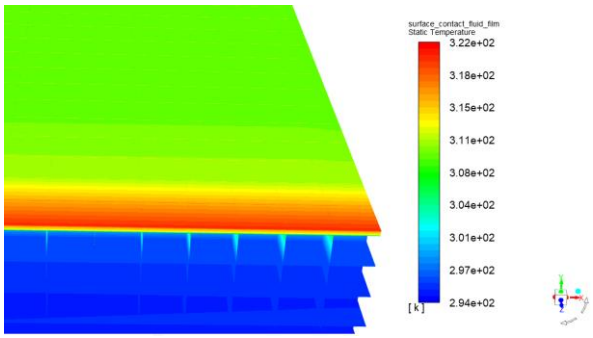

Fig. 12. Isometric view of a temperature distribution in the fluid up to contact surface with heating film, drawn on mesh facets.

Despite a denser mesh and good residual values, the temperature distribution (Fig. 12) shows remarks of not completely converged solution. It may be the result of the SIMPLE solver or not enough iterations. Since computational time was limited and residuals generally stable within range of 200 iterations, calculation was stopped, solver changed and results selected for validation after converging.

5 Conclusions

The main aim of the paper was to apply numerical calculations in ANSYS software to solve problems related to steady-state convective heat transfer during the cooling liquid flow in a minichannel heat sink. A mathematical model of fluid flow in a selected channel was proposed for the calculations. It was verified as a result of the experimental data. The essential element of the research stand was the test section with minichannels. The distribution of temperature on the surface of the heated outer wall surface of the minichannels was measured by an infrared camera. The fluid temperature and pressure at the inlet and outlet of the test section were also collected simultaneously.

A CAD model for calculations was prepared with respect to the geometry of the test section. The mesh was created in ANSYS Mesher with an optimization strategy to avoid averaging between the cells. The computational volume was limited to representation of the modeled minichannel and its surroundings to reduce the required power and time of calculations. Suitable model of turbulences was selected and materials temperature dependencies were considered to closely reproduce the behavior of fluid in experiments. The iterative process of creating the model and comparing the results obtained by the CFD calculation was used to capture the fluid behavior.

The results were presented graphically as the velocity magnitudes and temperature distributions as the main results from numerical calculations.

Acknowledgements

The research reported herein was supported by a grant from the National Science Centre, Poland, No. UMO-2018/31/B/ST8/01199.

References

1. S.G. Kandlikar, J. Heat Transf., **138**(2), 021504 (2016)
2. S.G. Kandlikar, Int. J. Therm. Sci. **49**(7), 1073-1085 (2010)
3. S.S. Bertsch, E.A. Groll, S.V. Garimella, Nanoscale Microscale Thermophys. Eng. **12**(3), 187-227 (2008)
4. D. F. Sempertegui-Tapia, G. Ribatski, Exp. Therm. Fluid Sc. **89**, 98-109 (2017)
5. R. Mastrullo, A. W. Mauro, J. R. Thome, G. P. Vanoli, L. Viscito, Int. J. Therm. Sci. **106** 1-17, (2016)
6. A. Krishnan, K. Balasubramanian, S. Suresh, Int. J. Heat Mass Transfer **120**, 1341-1357 (2018)
7. S.-M. Kim, I. Mudawar, Int. J. Heat Mass Transf. **77**, 627-652 (2014)
8. W. Qu, I. Mudawar, Int. J. Heat Mass Transf. **46**(15), 2755-2771 (2003)
9. G. Hestroni, A. Mosyak, Z. Segal, G. Ziskind, Int. J. Heat Mass Transf. **45** (6), 3275-3286 (2002)
10. B. Maciejewska, M. Piasecka, Int. J. Heat Mass Transf. **107**, 925–933 (2017)
11. B. Maciejewska, M. Piasecka, Heat Mass Transf. **53**, 1211–1224 (2017
12. K. Strąk, M. Piasecka, B. Maciejewska, Int. J. Heat Mass Transf. **117**, 375–387 (2018)
13. B. Maciejewska, K. Strak, M. Piasecka, Int. J. Numer. Methods Heat Fluid Flow **28**(1), 206–219 (2018)
14. B. Maciejewska, S. Błasiak, M. Piasecka, EPJ Web of Conf. **143**, 02071, 5 pages (2017)
15. B. Maciejewska, P. Łabędzki, A. Piasecki, M. Piasecka, EPJ Web of Conf. **143**, 02070, 5 pages (2017)
16. S. Blasiak, J. E. Takosoglu, P. A. Laski, In: *Eng. Mechanics*, Fuis V (ed), 96–99 (2014)
17. HAYNES, *HAYNES ® 230 ® alloy* (2019)
18. 3M Performance Materials, *3M Fluorinert™ Electronic Liquid FC-72*, 1–4 (2002)